PAPER

Rotation of nanoflake driven by strain gradient fields in locally-indented graphene

IOP Publishing Nanotechnology
Nanotechnology 31 (2020) 015303 (8pp) https://doi.org/10.1088/1361-6528/ab4441

Rotation of nanoflake driven by strain gradient fields in locally-indented graphene

Muhammad Bilal Khan[1,2,3], **Shuai Wang**[1,2,3], **Chao Wang**[4,5] and **Shaohua Chen**[1,2,3,5]

[1] Institute of Advanced Structure Technology, Beijing Institute of Technology, Beijing 100081, People's Republic of China
[2] Beijing Key Laboratory of Lightweight Multi-functional Composite Materials and Structures, Beijing Institute of Technology, Beijing, 100081, People's Republic of China
[3] Collaborative Innovation Center of Electric Vehicles in Beijing, Beijing Institute of Technology, Beijing, 100081, People's Republic of China
[4] LNM, Institute of Mechanics, Chinese Academy of Sciences, Beijing 100190, People's Republic of China

E-mail: wangchao@lnm.imech.ac.cn and shchen@bit.edu.cn

Received 14 July 2019, revised 13 August 2019
Accepted for publication 13 September 2019
Published 9 October 2019

Abstract

Rotation of nano-components is necessary in nanoscale mechanical systems (NMS) to enable various functions of nanomachines, however, the actuation and modulation of nanoscale rotation have been poorly investigated up to now. In this paper, we conduct molecular dynamics simulations to study the in-plane rotation of a graphene nanoflake hinged to a graphene substrate by easily accessible nanoindentation techniques. The flake can be driven to rotate by strain gradient fields (SGFs) induced by indenting the substrate locally. The effect of flake size, indenting velocity and position on flake rotation are studied systematically. It is found that there exists a critical range of flake size which is comparable to that of SGFs. The direction of flake rotation, i.e. clockwise or counterclockwise, can be tuned effectively by indenting the substrate asymmetrically with respect to the flake. Besides, the rotation can be speeded up by simply indenting more quickly. Furthermore, the flake can be trapped in a desired region on the substrate by adopting double SGFs. The continuous rotation of the flake can be realized by intermittently indenting the substrate near the flake. These results may be useful for designing the rotation of components in NMSs and nanoscale manipulation.

Supplementary material for this article is available online

Keywords: strain gradient field, graphene substrate, nano-rotation, nano-indenting, molecular dynamic simulations

(Some figures may appear in colour only in the online journal)

1. Introduction

Motion (translation/rotation) regulation is a fundamental requirement for the working of machinery. At the macroscopic level, components like gear pair, crank slider and cam are used to regulate the mechanical motion to enable various functions of machines in practical applications. With the development of nanotechnology, the regulation of nanoscale motion has received increasing attention from both scientific and engineering fields in recent years due to its scientific richness and basic importance in vast applications of nanoscale mechanical systems (NMS). A series of manipulation schemes have been proposed to actuate the motion of nano-objects based on the gradient of curvature [1, 2], strain [3, 4], stiffness [5], surface chemistry [6] and structural surface design [7, 8] of the substrate as well as applied voltage [9–11], electric current [12, 13], thermal energy [14–19], asymmetrically chemical interactions [20–23]. These previous

[5] Authors to whom any correspondence should be addressed.

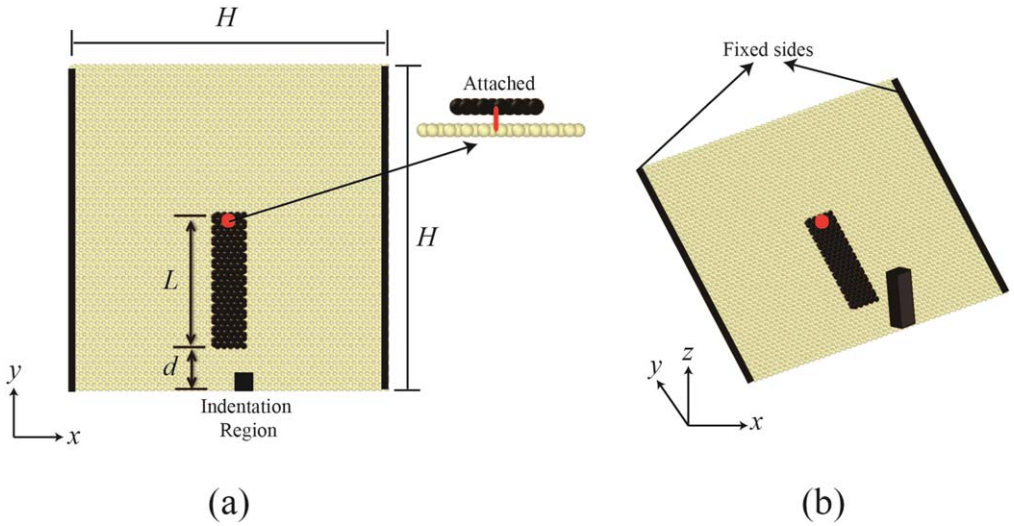

Figure 1. The schematic model of a rectangle graphene nanoflake hinged on a square graphene substrate with $H = 12$ nm, $L = 5$ nm and $d = 1.6$ nm. (a) the top view; (b) the perspective view.

studies mainly focus on the actuating mechanisms of translational motion. Only a few of these studies [9, 10] address the actuation of large rotational motion using the specific superlubricity of multi-walled structure of CNT. For example, Fennimore *et al* [9] reported a voltage-driven nanoscale electromechanical actuator incorporating a rotatable metal plate, with a multi-walled carbon nanotube serving as the key motion-enabling element.

However, considering the diverse requirements in practical applications, more intensive research is still needed to explore an effective way to manipulate nanoscale rotation. It has been reported that a controllable strain gradient field can be induced in the graphene substrate pressed by the tip of an atomic force microscope (AFM) [24] or by the pillars of nano structured surfaces [25, 26]. Meanwhile, it has been addressed that nanoscale objects can be driven to move translationally and/or rotationally by strain gradient fields in both theoretical and experimental studies [3, 4, 27]. Based on the above knowledge, we propose that it is possible to use nanoindentation techniques to realize nanoscale rotation.

In this paper, using full-atomic molecular dynamics (FAMD) simulations, we study the in-plane rotation of a nanoflake hinged on a graphene substrate under nanoscale indentation. The effect of magnitude of indenting velocity, maximum indenting displacement, the distance between the indenting point and flake, and flake size on its rotation has been investigated systematically. According to our results, we further propose several methods to effectively control the flake rotation on the substrate, including changing the rotation direction, driving the flake to rotate constantly or stop at a desired region by obstacles or making traps in substrate. The results should be useful for the design of manipulation techniques for nanoscale rotation in NMSs.

The rest of this paper is organized as follows: the numerical model of nanoscale rotational motion as well as the methodology are given in section 2. The driving mechanisms and main influencing factors are discussed in detail and some controlling methods are addressed in section 3. The results are concluded at the end of this paper.

2. Simulation Model

Considering that graphene is one of the most typical and well-studied 2D material with a smooth surface, the force field function for molecular dynamic simulations of which is widely used and easily accessible, we chose it as the main part of our numerical model. As shown in figure 1(a), the numerical model of the nanoscale rotation system is composed of a square graphene sheet (12×12 nm) as the substrate and a rectangle graphene flake (1×5 nm) as the rotating part attaching itself tightly to the substrate with the equilibrated distance of 0.34 nm. The graphene flake can only rotate around the red dot, which is hinged to the center of substrate like a mechanical bearing. The hinge can usually be realized by using functional groups [28], doping [29, 30] or multi-walled carbon nanotube as rotation-enabling element [9, 10] experimentally. Other parts of the flake are set free and far enough from the edge of the substrate to eliminate boundary effects. The substrate is pre-tensioned to a strain of 0.02 and remains in the tensioned state by fixing the two opposite sides (black regions) in all simulations to avoid wrinkle effects [31, 32]. The other part of the substrate is left free. Then, the substrate is indented with a constant indenting velocity at the black square spot labeled as 'Indentation Region' in figure 1(a). The perspective view of numerical system is given in figure 1(b). It is similar to the experimental scheme [24] where a graphene membrane is suspended over open holes and indented by an atomic force microscope (AFM) to measure the mechanical properties of monolayer graphene membranes.

All the simulations were carried out on open source software large-scale atomic/molecular massively parallel simulator (LAMMPS) [33]. The interlayer van der Waals interaction between the flake and the substrate is modeled on

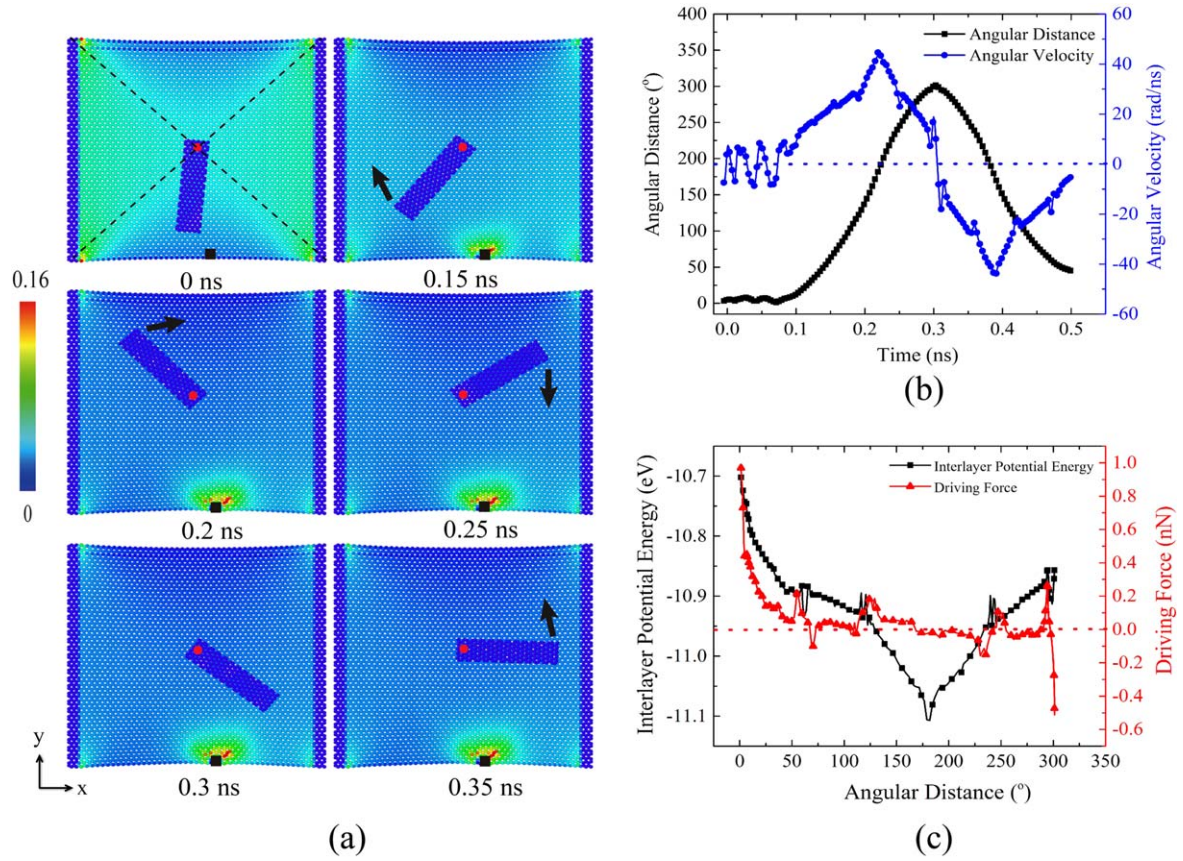

Figure 2. The in-plane rotation of a nanoflake on a locally indented substrate with strain gradient field. (a) The typical snapshots of the rotating flake on the substrate with non-uniform local strain indicated by color; (b) the angular velocity and rotating angle of the flake as the elapsed time; (c) the variation of the potential energy of the flake as well as the driving force on the flake in rotation. The small square black region is the indented point.

the Lennards-Jones 12-6 potential $\varphi(r) = 4\varepsilon[(\sigma/r)^{12}\text{-}(\sigma/r)^{6}]$, where ε is depth of potential well of 2.96 meV, σ is the zero energy distance of 0.3407 nm and r is the distance between two particles. The AIREBO force field was used to define the covalent bond C–C interaction between the graphene layers (substrate and flake). The time step was 1 fs. The system is initially relaxed at 300 K using NVT ensemble and then NVE (N is number of atoms, V is volume, T is temperature, E is the total energy) ensemble is adopted to simulate the motion behavior of the flake on the substrate. The temperature of the substrate was kept at 300 K. The indentation is simulated by the function $F(r) = K(r\text{-}R)^2$ where K is a specified force constant indicating the stiffness of the indenter, R is the position of the plane and r-R is the distance from the plane. See the command 'fix indent' in LAMMPS. The strain of the substrate is defined as $\varepsilon = \varepsilon_x + \varepsilon_y$, where $\varepsilon_i = (l_i - l_{i0})/l_{i0}$, $i = x$ or y, and l_i and l_{i0} are the current and initial distance of neighboring atoms in the substrate.

3. Results and discussion

3.1. Flake motion and mechanism

Figure 2(a) shows typical snapshots in the period of actuation, clockwise and anticlockwise rotation of the flake as the substrate is indented constantly. At the initial time, although the system is well equilibrated, the deformation of the four areas separated by the two diagonal dotted lines in the substrate is obviously non-uniform due to the restriction of the two fixed sides, the strain in the top and bottom areas is smaller while that in the left and right ones is larger as indicated by color. The definition of the local strain in the substrate is given in section 2. The flake stands still initially in the bottom region in the substrate, then, the black square region near the front edge of the substrate is indented along z-axis (out-of-plane) with an indenting velocity of 0.1 m s^{-1}, which induces an obvious SGF around the indenting point as indicated by the color map in the snapshot at 0.15 ns. The strain magnitude of the SGF decreases as it is away from the indenting point. The flake stays still before 0.15 ns due to a weaker SGF that induces a negligible driving force on the flake. As the substrate is further indented at 0.15 ns, both the functional area and the strain magnitude of SGF increase, and the flake gradually rotates away from the higher-strain region. This can be explained according to previous studies [3, 4] on the SGF of graphene: the flake on the graphene substrate with larger tensile strain would have higher potential energy, so a gradient of the potential energy, i.e. a force, would be induced on the flake as it lies in a SGF, furthermore in this model, due to the inner end of the flake being hinged to the substrate, a

torque would be generated, which makes the flake rotate away from the indenting region. The flake will continue to rotate to the maximum angle as shown at 0.2, 0.25 and 0.3 ns. As the flake enters into the SGF from the other side, the induced force on the flake by the strain gradient acts as resistance making the flake slow down and stop for some time. Then, the flake is driven to rotate back anticlockwise at 0.35 ns. Afterwards, the flake will continue to rotate clockwise and counterclockwise between the initial and final region because of the inertia and less friction, and eventually it will stop at the low strain region ∼180° away from the indenting point. The whole rotation of flake can be seen in movie 1, available online at stacks.iop.org/NANO/31/015303/mmedia in supporting materials. Figure 2(b) shows the angular velocity and the rotating degree of the flake. The angular velocity fluctuates around zero until ∼0.13 ns when the strain gradient of the SGF grows large enough, then it increases constantly to the maximum at ∼0.23 ns when the flake reaches to the low strain region ∼180° away from the starting point with the maximum angular velocity of ∼41 rad s^{-1}. After that, it starts decreasing gradually to zero as the flake again reaches the SGF with the maximum rotating degree of 300°, and then it starts increasing in a counterclockwise direction with a negative value. We further calculate the driving force exerted by the substrate on the flake as well as the interlayer potential energy between them as shown in figure 2(c). The flake has a minimum potential energy as it locates in the region of ∼180° away from the initial point due to the nearly zero strain gradient there. The exerted force on the flake before this point is nearly positive indicating the driving nature, and it becomes negative after the point showing the resistance nature. In addition, at the four positions with the angles about 60°, 125°, 240° and 300° away from the initial point, the potential energy fluctuates drastically due to the obvious SGFs originated from the restriction of the two fixed boundaries.

Here, we noted that, for the candidate of graphene, other kinds of 2D materials like hexagonal boron nitride [34] and Boron carbon nitride [35], which have similar smooth structure to graphene, are more likely to be used as basic components of the model system than other 2D materials like chalcogenides (MoS_2, WS_2 and $MoSe_2$) [36] and metal oxides (MoO_3, WO_3 and TiO_2) [37] with relatively rough and complex in-plane structures.

3.2. Effect of flake size, indenting position, velocity and magnitude

To investigate the effect of flake size on rotation, we tune the length-to-width ratio of the flake in a wide range of 0.8–11 for a given length of 5 nm and keep all other settings constant. We find that the continuous flake rotation can be realized only when the ratio falls into the range of 0.8–11 and the minimum strain gradient value needed to rotate the flake increases with flake size as shown in figure S2, the larger flake can be driven to rotate continuously with comparatively larger strain gradient value. Figure 3 gives two extreme cases that the ratio is out of the range, e.g., equal to 0.8 and 11. When the ratio is 0.8, as shown in figure 3(a) and movie 2 in the supporting materials, the large flake only rearranges itself slightly (equal to θ in figure 3(a)) without continuous rotation as indenting the substrate. This can be attributed to the larger friction between a bigger flake and the substrate and remarkable wrinkles forming in a big flake as shown in figure S3. Here we noted that wrinkles, in either the substrate or the flake, would have a big resistance to the rotation of the flake, that is why we set a pre-tension strain of 0.02 in the substrate in all our simulations. When the ratio equals 11, as shown in figure 3(b) and movie 3, the flake is so narrow compared to the width of the SGF activated in the substrate that it could not feel the strain gradient, as a result, it behaves like a rope due to the reduced bending stiffness and bends easily along with the curvature of the indented substrate.

Figures 4(a), (b) shows that the rotating direction of the flake can be tuned effectively clockwise or counterclockwise by applying an asymmetric indentation, i.e., as the right area of the substrate is indented, as the black square shows in figure 4(a), the flake rotates clockwise, while the flake rotates counterclockwise as the left area of the substrate is indented. If we indent the substrate symmetrically from the point aligned to the center axis of the flake, it is unpredictable because the flake may rotate clockwise or counterclockwise or may not rotate due to a symmetric force induced by the strain gradient in the substrate. Besides, the distance between the indenting point and the flake should also be chosen carefully. We gradually move the indenting point away from the flake edge and find the critical distance is ∼2.5 nm, beyond which the flake cannot be driven to rotate. This is because the strain gradient field induced by the indentation decays gradually to zero as it is ∼2.5 nm away from the indentation point as shown in figure S4. As shown in figure 4(c), if the indenting point is 3.2 nm away from the flake, it cannot feel the strain gradient induced by continuous indentation and keeps still even the substrate is indented to be broken (see movie 4 in the supporting materials for the vivid process).

We also study the effect of indenting velocity on flake rotation. As shown in figure 5(a), we find that if the indenting point is ∼1 nm away from the flake, the maximal angular velocity of the flake would increase as the substrate is indented more quickly from ∼0.01–0.25 m s^{-1} and less time will be used for the flake to reach the maximum angle of 300°; but if the indenting point is close to the flake, e.g. 0.3 nm, the flake cannot rotate as a smaller indenting velocity of 0.05 m s^{-1} is applied as shown in movie 5, because in this case, the flake has more time to adjust itself to become symmetric with the point of indentation, which results in a negligible moment of force on the flake and leads to its failure of rotation. The indenter velocity should not be larger than 0.3 m s^{-1}, otherwise the substrate would be indented to break. We also study the effect of the indenting distance varying from ∼0.5–3.0 nm on the flake rotation with a constant indenting velocity of 0.1 m s^{-1} as shown in figure 5(b). The flake cannot rotate when the substrate is indented a distance smaller than 0.9 nm due to a minor SGF induced in the substrate as expected. The increase of indenting distance from 0.9–2.0 nm will increase the angular velocity of the flake with

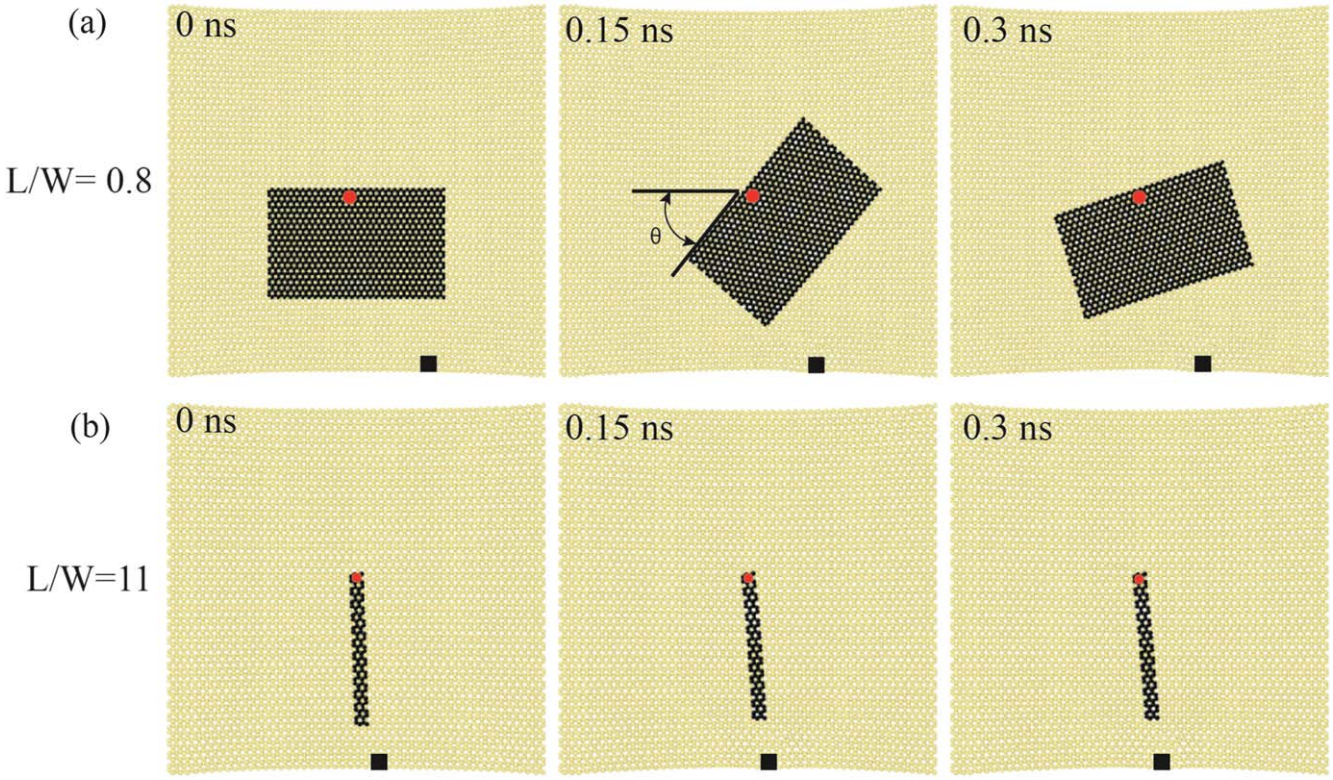

Figure 3. The effect of the flake size on its rotation. The length-to-width ratio is (a) 0.8 and (b) 11.

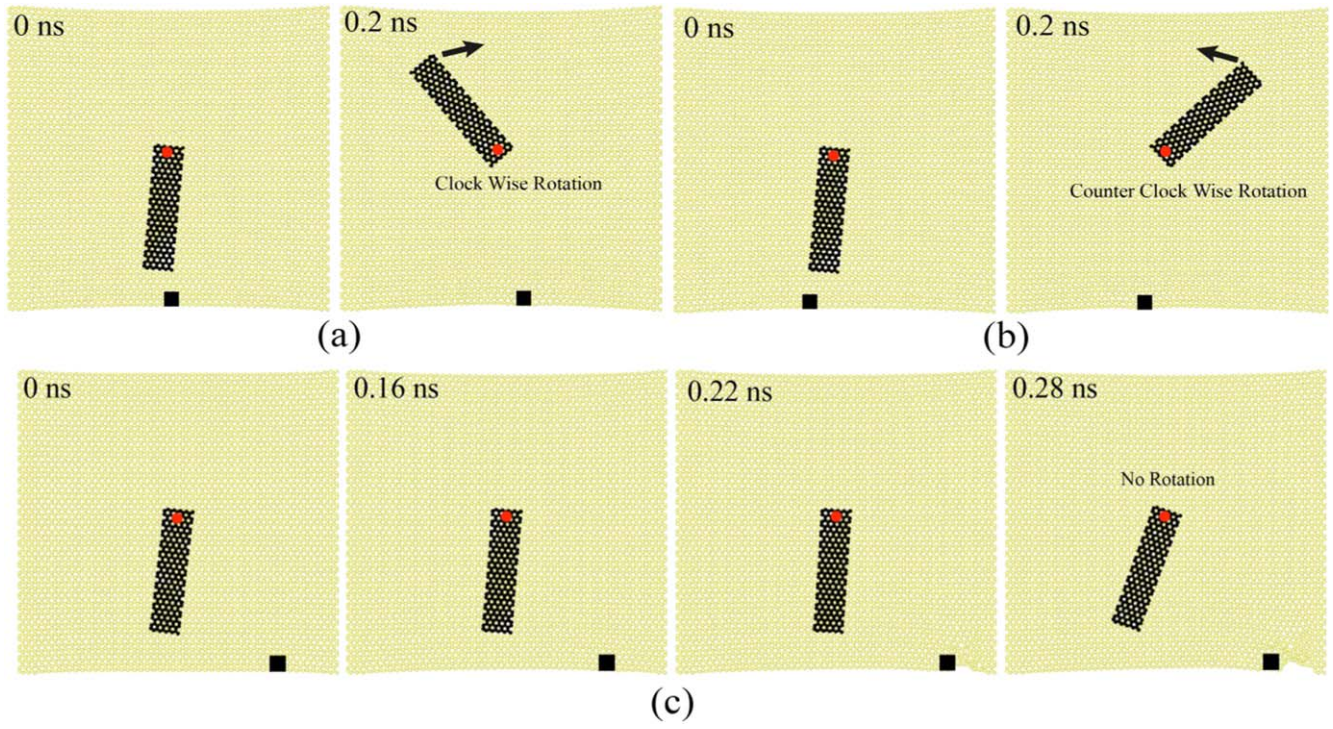

Figure 4. The effect of indenting position on flake rotation. The indenting point is on the (a) right and (b) left of the flake; (c) the indenting point is 3.2 nm away from flake.

the decreased time to reach the maximum angle of 300° due to the enhanced SGF in the substrate; for larger indented distance, it will not have any effect on angular velocity of flake and time to reach the maximum angular distance. The substrate would be indented to break if the indenting distance is larger than 2.5 nm. It is found that a suitable indenting distance is in the range of 0.9–2.4 nm to ensure a smooth rotation of the flake by a series of simulations. In addition, we

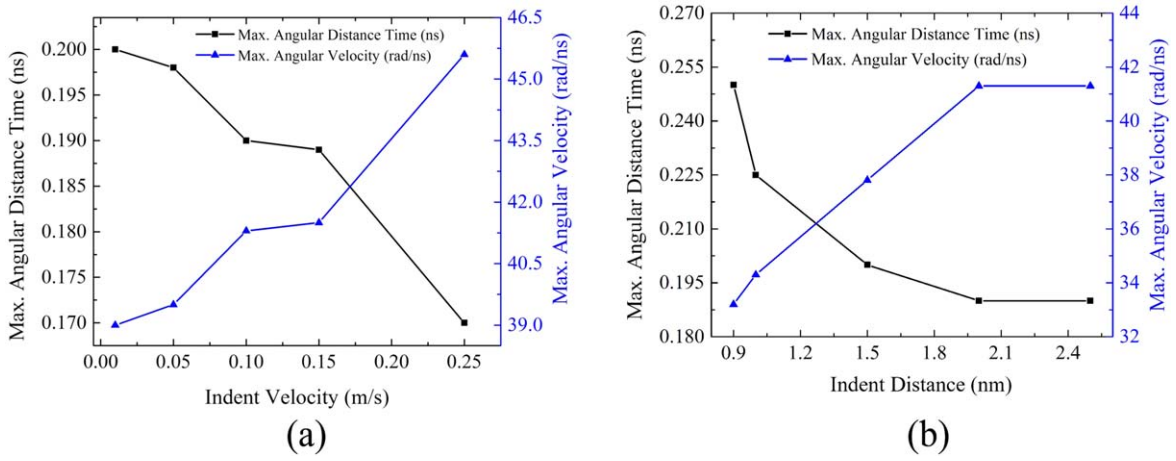

Figure 5. Effect of indenting velocity (a) and indenting distance (b) on flake rotation.

also examine the effect of the area of indentation from 1–9 nm^2 and find that the flake rotation is independent of the indenting area as long as the conditions mentioned above are satisfied as shown in figure S5.

The effect of thermal fluctuation on flake rotation has also been investigated by setting a variable simulation temperature from 100 and 500 K. Different from the continuous rotation of flake as shown in figure 2, both the flake and substrate fluctuate drastically if a higher temperature, e.g., 400 or 500 K is adopted. During indentation, the flake just deviates from the initial position and then keeps fluctuating there as shown in movie 7 in the supporting information. This is easily understood: from figure 2(c), the maximum directional driving force of flake rotation at 300 K can be obtained ~4.2 pN/atom, i.e., 1 nN divided by the number of atoms in the flake, 240 here. As the temperature increases the directional driving force should be disturbed by the thermal fluctuations of both the flake and the substrate due to the random nature of thermal fluctuations.

3.3. Further control of flake rotation

Based on the understanding of underlying mechanisms and basic tuning skills discussed above, further manipulating techniques are proposed in the following part to facilitate potential applications. As shown in figure 6(a), two local regions indicated by black and green are indented to produce two SGFs on the substrate to restrain flake rotation in an assigned narrow region. As discussed above, the flake is activated at the first indenting region (black) to rotate forward at 0 ns, as it enters into the second indenting region at 0.18 ns, it does not move forward and stops for a fraction of time and returns back to the initial indentation point at 0.35 ns and then continues to rotate between the initial and desired point, see movie 6 in the supporting materials. By making the two indenting points closer, the flake can be trapped and stopped there precisely as shown in figure S6. The flake can also be pinned at a desired position by setting a small piece of graphene sheet, or other nanoparticles fixed in the path on the substrate, as a nanoscale obstacle. As shown in figure 6(b), the flake starts to rotate and strikes the obstacle, but different from its behavior near a SGF, it rebounds back and forth near the obstacle at ~0.28–0.30 ns, and eventually it stops nearby, see movie 8 in the supporting materials. In experiments, we can use a technique such as AFM probe lingering at any point on the substrate as an obstacle to stop the rotating flake without indentation. The continuous rotation of the flake on the substrate in a clockwise or counterclockwise can be achieved by indenting the region near the free end of the flake constantly as shown in figure 6(c). After initial indentation when the flake starts rotating, we remove the initial indenter and let the flake rotate continuously in a circular motion with inertia, when its angular velocity gradually decreases to zero, we can again use the indenter to start its rotation, and by this method, the flake will rotate continuously in circular motion. This method can be used experimentally by nano indenter [38–40] or similar mechanisms to AFM probe.

4. Conclusion

We study the in-plane rotation of a graphene nanoflake hinged to the center of a graphene substrate using the full-atom molecular dynamics simulations. The pre-tensioned substrate with 0.02 strain is indented locally by a virtual indenter to deform out-of-plane, which induces a SGF in the substrate. The hinged flake is driven to rotate by the gradient of potential energy in SGF. The rotation of the flake is affected by the size, indenting velocity, indenting position and the distance to which the substrate is pulled down. The flake would not be driven to rotate if it is too wide ($L/W \geqslant 11$) or too narrow ($L/W < 0.8$). The maximal angular velocity of the flake would increase as the substrate is indented more quickly from ~0.01–0.25 $m\,s^{-1}$ when the indenting point is ~1 nm away from the flake and less time will be used for the flake to reach the maximum angle of 300°; the substrate would break when the indenting velocity is as high as 0.3 $m\,s^{-1}$. The flake would not rotate if the substrate is indented slightly, e.g. 0.5 nm. The maximum angular velocity of the flake increases as the time needed to achieve the maximum angle of 300° decreases. When the indenting depth

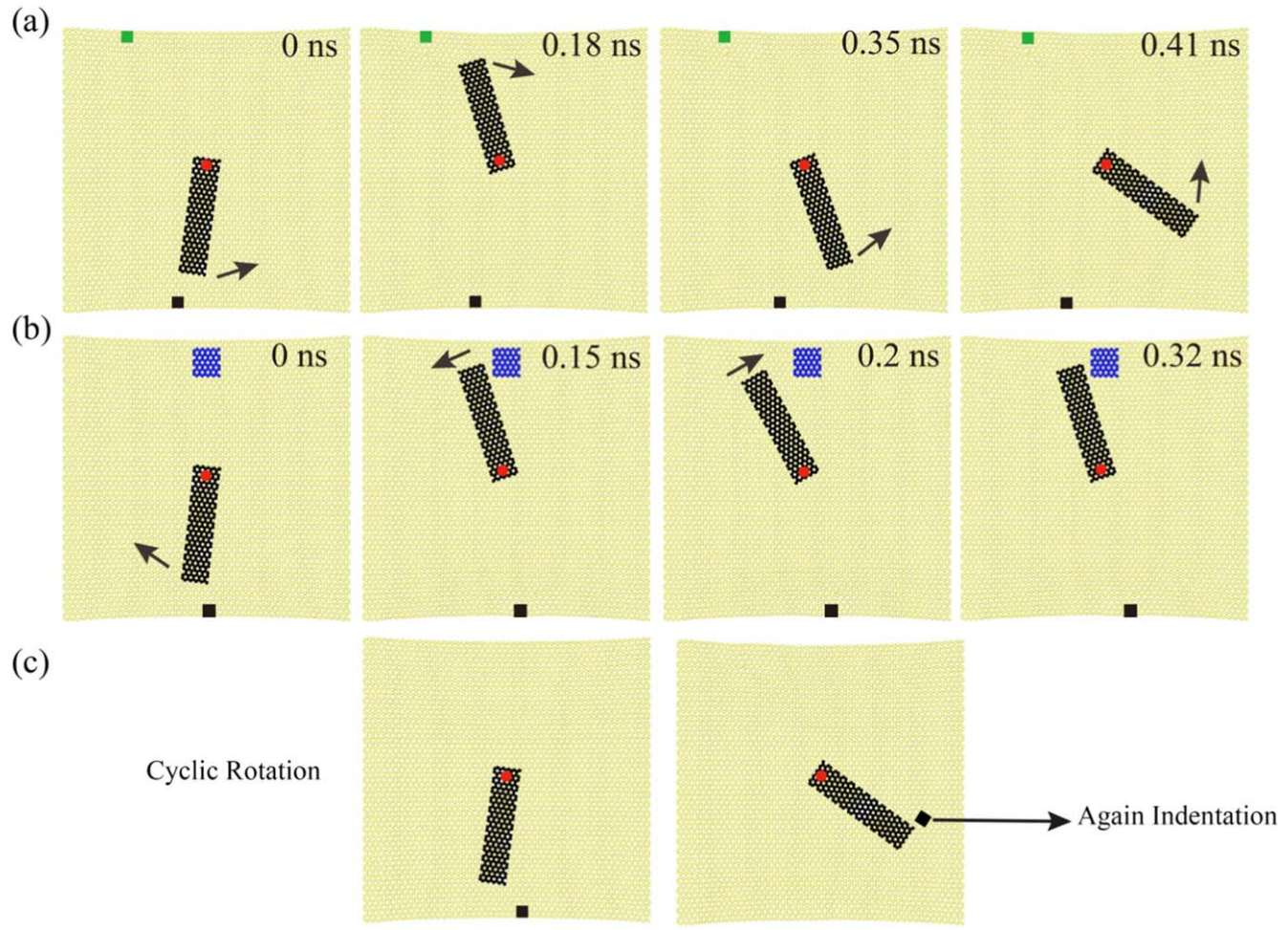

Figure 6. Further control of flake rotation. (a) The flake rotation is restrained in a tunable region by two indenting points labeled black and green; (b) the flake is stopped by a graphene sheet as an obstacle; (c) the flake is driven to rotate continuously by intermittently indenting the region near the free end of the flake.

increases from ∼0.9–2 nm, it will not have any effect on the flake rotation as the substrate is further indented. The substrate breaks when the indented distance is greater than 2.5 nm. The area of indentation does not affect the rotation of the flake. The clockwise or counterclockwise rotation of the flake can be tuned effectively by the indenting position with respect to the flake. The motion of the flake can be restricted to the desired point or region on the substrate by using two SGFs or nano-obstacles. The continuous rotation of the flake can be realized by constantly indenting the substrate near the flake. These results may be useful for the design of the rotation in NMSs and nanoscale manipulation.

Acknowledgments

The work reported here is supported by NSFC through Grants Nos. 11372317, 11532013 and 11602270 and the CAS/SAFEA International Partnership Program for Creative Research Teams.

Author contributions

S H C and C W conceived the original idea, designed and supervised the simulations. M B K formulated the numerical model, conducted all simulations and drafted the paper. C W revised the manuscript. All authors reviewed and contributed to the paper.

Competing financial interests

The authors declare no competing interests.

ORCID iDs

Chao Wang https://orcid.org/0000-0002-3234-6917

References

[1] Lv C, Chen C, Chuang Y-C, Tseng F-G, Yin Y, Grey F and Zheng Q 2014 Substrate curvature gradient drives rapid droplet motion *Phys. Rev. Lett.* **113** 026101

[2] Dai C, Guo Z, Shang H and Chang T 2016 A nanoscale linear-to-linear motion converter of graphene *Nanoscale* **8** 14406–10

[3] Huang Y, Zhu S and Li T 2014 Directional transport of molecular mass on graphene by straining *Extreme Mech. Lett.* **1** 83–9

[4] Wang C and Chen S H 2015 Motion driven by strain gradient fields *Sci. Rep.* **5** 13675

[5] Chang T, Zhang H, Guo Z, Guo X and Gao H 2015 Nanoscale directional motion towards regions of stiffness *Phys. Rev. Lett.* **114** 015504

[6] Wang J and Manesh K M 2010 Motion control at the nanoscale *Small* **6** 338–45

[7] Ghorbanfekr-Kalashami H, peeters F M, Novoselov K S and Neek-Amal M 2017 Spatial design and control of graphene flake motion *Phys. Rev.* B **96** 060101

[8] Peymanirad F, Singh S K, Ghorbanfekr-Kalashami H, Novoselov K S, Peeters F M and Neek-Amal M 2017 Thermal activated rotation of graphene flake on graphene *2D Mater.* **4** 025015

[9] Fennimore A M, Yuzvinsky T D, Han W-Q, Fuhrer M S, Cumings J and Zettl A 2003 Rotational actuators based on carbon nanotubes *Nature* **424** 408–10

[10] Bailey S W, Amanatidis I and Lambert C J 2008 Carbon nanotube electron windmills: a novel design for nanomotors *Phys. Rev. Lett.* **100** 256802

[11] Shklyaev O E, Mockensturm E and Crespi V H 2013 Theory of carbomorph cycles *Phys. Rev. Lett.* **110** 156803

[12] Regan B C, Aloni S, Ritchie R O, Dahmen U and Zettl A 2004 Carbon nanotubes as nanoscale mass conveyors *Nature* **428** 924–7

[13] Dundas D, McEniry E J and Todorov T N 2009 Current-driven atomic waterwheels *Nat. Nanotechnol.* **4** 99–102

[14] Barreiro A, Rurali R, Hernández E R, Moser J, Pichler T, Forró L and Bachtold A 2008 Subnanometer motion of cargoes driven by thermal gradients along carbon nanotubes *Science* **320** 775–8

[15] Schoen P A E, Walther J H, Poulikakos D and Koumoutsakos P 2007 Phonon assisted thermophoretic motion of gold nanoparticles inside carbon nanotubes *Appl. Phys. Lett.* **90** 253116

[16] Chang T and Guo Z 2010 Temperature-induced reversible dominoes in carbon nanotubes *Nano Lett.* **10** 3490–3

[17] Becton M and Wang X Q 2014 Thermal gradients on graphene to drive nanoflake motion *J. Chem. Theory Comput.* **10** 722–30

[18] Somada H, Hirahara K, Akita S and Nakayama Y 2009 A molecular linear motor consisting of carbon nanotubes *Nano Lett.* **9** 62–5

[19] Shanahan M E and Sefiane K 2014 Recalcitrant bubbles *Sci. Rep.* **4** 4727

[20] Bain C D, Burnett-Hall G D and Montgomerie R R 1994 Rapid motion of liquid drops *Nature* **372** 414–5

[21] Dos Santos F D and Ondarcuhu T 1995 Free-running droplets *Phys. Rev. Lett.* **75** 2972

[22] Shanahan M E 1990 Capillary movement of nearly axisymmetric sessile drops *J. Phys. D: Appl. Phys.* **23** 321–7

[23] Shanahan M E and de Gennes P-G 1997 Start-up of a reactive droplet *Comptes Rendus de l'Académie des Sciences-Series IIB-Mechanics-Physics-Chemistry-Astronomy* **324** 261–8

[24] Lee C *et al* 2008 Measurement of the elastic properties and intrinsic strength of monolayer graphene *Science* **321** 385–8

[25] Neek-Amal M and Peeters F M 2012 Strain-engineered graphene through a nanostructured substrate. I. Deformations *Phys. Rev.* B **85** 195445

[26] Neek-Amal M, Covaci L and Peeters F M 2012 Nanoengineered nonuniform strain in graphene using nanopillars *Phys. Rev.* B **86** 041405

[27] Nabarro F R N 1987 *Theory of Crystal Dislocations* (New York: Dover)

[28] Lee D W, De Los Santos L, Seo J W, Leon Felix L, Bustamante D A, Cole J M and Barnes C H W 2010 The structure of graphite oxide: investigation of its surface chemical groups *J. Phys. Chem.* B **114** 5723–8

[29] Wu Z S, Ren W, Xu L, Li F and Cheng H M 2011 Doped graphene sheets as anode materials with superhigh rate and large capacity for lithium ion batteries *ACS Nano* **5** 5463–71

[30] Long D H, Li W, Ling L, Miyawaki J, Mochida I and Yoon S-H 2010 Preparation of nitrogen-doped graphene sheets by a combined chemical and hydrothermal reduction of graphene oxide *Langmuir* **26** 16096–102

[31] Zheng Q B *et al* 2010 Effects of functional groups on the mechanical and wrinkling properties of graphene sheets *Carbon* **48** 4315–22

[32] Zhu W J, Low T, Perebeinos V, Bol A A, Zhu Y, Yan H, Tersoff J and Avouris P 2012 Structure and electronic transport in graphene wrinkles *Nano Lett.* **12** 3431–6

[33] Hardy R J 1982 Formulas for determining local properties in molecular-dynamics simulations: shock waves *J. Chem. Phys.* **76** 622–8

[34] Wang H, Zhao Y, Xie Y, Ma X and Zhang X 2017 Recent progress in synthesis of two-dimensional hexagonal boron nitride *J. Semicond.* **38** 031003

[35] Ci L *et al* 2010 Atomic layers of hybridized boron nitride and graphene domains *Nat. Mater.* **9** 430

[36] Li X *et al* 2017 Graphene and related two-dimensional materials: Structure-property relationships for electronics and optoelectronics *Appl. Phys. Rev.* **4** 021306

[37] Sun Z *et al* 2014 Generalized self-assembly of scalable two-dimensional transition metal oxide nanosheets *Nat. Commun.* **5** 3813

[38] Das B, Prasad K E, Ramamurty U and Rao C N R 2009 Nano-indentation studies on polymer matrix composites reinforced by few-layer graphene *Nanotechnology* **20** 125705

[39] Zhang Y P and Pan C X 2012 Measurements of mechanical properties and number of layers of graphene from nano-indentation *Diamond Relat. Mater.* **24** 1–5

[40] Shokrieh M M, Hosseinkhani M R, Naimi-Jamal M R and Tourani H 2013 Nanoindentation and nanoscratch investigations on graphene-based nanocomposites *Polym. Test* **32** 45–51